# Response of Southern Ocean circulation to global warming may enhance basal ice shelf melting around Antarctica

**Tore Hattermann · Anders Levermann**

**Abstract** We investigate the large-scale oceanic features determining the future ice shelf–ocean interaction by analyzing global warming experiments in a coarse resolution climate model with a comprehensive ocean component. Heat and freshwater fluxes from basal ice shelf melting (ISM) are parameterized following Beckmann and Goosse [Ocean Model 5(2):157–170, 2003]. Melting sensitivities to the oceanic temperature outside of the ice shelf cavities are varied from linear to quadratic (Holland et al. in J Clim 21, 2008). In 1% per year $CO_2$-increase experiments the total freshwater flux from ISM triples to 0.09 Sv in the linear case and more than quadruples to 0.15 Sv in the quadratic case after 140 years at which $4 \times 280$ ppm = 1,120 ppm was reached. Due to the long response time of subsurface temperature anomalies, ISM thereafter increases drastically, if $CO_2$ concentrations are kept constant at 1,120 ppm. Varying strength of the Antarctic circumpolar current (ACC) is crucial for ISM increase, because southward advection of heat dominates the warming along the Antarctic coast. On centennial timescales the ACC accelerates due to deep ocean warming north of the current, caused by mixing of heat along isopycnals in the Southern Ocean (SO) outcropping regions. In contrast to previous studies we find an initial weakening of the ACC during the first 150 years of warming. This purely baroclinic effect is due to a freshening in the SO which is consistent with present observations. Comparison with simulations with diagnosed ISM but without its influence on the ocean circulation reveal a number of ISM-related feedbacks, of which a negative ISM-feedback, due to the ISM-related local oceanic cooling, is the dominant one.

## 1 Introduction

The unique zonally unblocked topography in the Southern Ocean (SO) gives rise to the Antarctic circumpolar current (ACC), the strongest oceanic circulation on Earth. Connecting the Atlantic, Pacific and Indian basin, it is on the one hand a major contributor to worldwide ocean ventilation. On the other hand, the strong and deep reaching zonal current is limiting the meridional oceanic transport. Therefore, it partly isolates the ocean south of the current from the northern circulation (England 1993; Rintoul et al. 2001).

The zonal momentum of the ACC is balanced by several forces. According to Borowski et al. (2002), the largest contribution is geostrophic, due to a meridional pressure gradient across the current. The pressure gradient arises from surface displacement (barotropic), as well as from the internal density distribution (baroclinic). Although wind stress induces strong zonal momentum at the surface, it cannot accelerate the water further down in the ocean because of blocked geopotential contours. Instead, it contributes indirectly to the geostrophic component via meridional Ekman transport as discussed extensively by, e.g. Olbers et al. (2004, 2006) and Gent et al. (2001). Model studies indicate that global warming will enhance the meridional density gradient and strengthen the current (Bi et al. 2002). According to recent observations, rising atmospheric temperatures may have already caused a warming of the deep ocean within the ACC (Böning et al. 2008; Gille 2002).

T. Hattermann (✉) · A. Levermann
Earth System Analysis,
Potsdam Institute for Climate Impact Research,
Potsdam University, Telegrafenberg A62,
14473 Potsdam, Germany
e-mail: tore.hattermann@pik-potsdam.de; toreh@gmx.net

The processes responsible for a meridional transport across the ACC are still poorly understood but seem to be caused by eddy diffusive processes and the meridional component of the predominantly zonal flow (Olbers et al. 2004). A main energy source for mixing is the density gradient across the ACC which is hence correlated to the strength of the geostrophic current itself. Thus, the ACC strength plays an important role in determining the heat budget of the SO.

South of the ACC, Circumpolar Deep Water is mixed with the coastal water masses in the currents of the large Southern Hemisphere Subpolar Gyres in the Ross and Weddell Sea (SPGs hereafter) (Bergamasco et al. 2002; Schröder and Fahrbach 1999; Gill 1972). In these regimes, deep and bottom water is formed (Orsi et al. 1999), and heat is transported towards the Antarctic continent.

With an area of $1.5 \times 10^6$ km$^2$, approximately 40% of the Antarctic continental shelf is covered by massive floating ice shelves, acting as a lid on the ocean. This causes a complex circulation system within submarine cavities (Williams et al. 1998). The presence of Antarctic ice shelves is considered to influence the flow speed of the adjacent continental ice (Scambos et al. 2004; Rignot et al. 2004). Observations, as well as numerical models, show that the amount of ice shelf melting (ISM) is crucial for the mass balance of ice shelves and might be strongly sensitive to climate change (Walker and Holland 2007; Rignot and Jacobs 2002; Williams et al. 2001). Moreover, the hydrology around the Antarctic continent is strongly affected by the interaction with the floating ice (Saenko and Weaver 2004) and varying saltwater fluxes in the SO may have caused significant changes in the global ocean circulation (Jacobs et al. 2002) in the past. Within the last decades, regional atmospheric and oceanographic changes in the SO have been observed (Jacobs et al. 2002). In the future, the interaction of different processes, e.g. ocean warming (Böning et al. 2008), increasing precipitation (Thomas et al. 2008), varying sea ice cover (Curran et al. 2003; Cavalieri et al. 2003) and melting of the Antarctic ice sheet and shelves (Alley et al. 2005), might reveal internal feedback mechanisms that influence the global climate system as a whole (Swingedouw et al. 2008a, b).

Various attempts have been made to understand the ice shelf–ocean interaction by using regional high resolution models (Holland et al. 2008; Smedsrud et al. 2006; Grosfeld and Sandhäger 2004; Lange et al. 2005). In combination with observations, these studies have provided a fair understanding of the different processes that govern basal ISM on a local scale. In addition, ISM seems to have considerable influence on large scale ocean circulation (Losch 2008) and several studies have proposed that oceanic warming is the reason for increasing mass loss from the grounded Antarctic ice sheet (Payne et al. 2004).

However, very little is known about the link between rising atmospheric temperatures and increasing ISM, because the sub-shelf cavity circulation is connected to the ocean at great depth. Moreover, the inclusion of ISM in global circulation models (GCMs) is hampered by incompatibility of grid sizes and complex boundary conditions. To our knowledge, there are no studies that focus on the effects of varying ISM in coupled global warming simulations.

Here we combine the coupled global climate model CLIMBER-3α with a coarse resolution ISM parameterization as introduced by Beckmann and Goosse (2003) and generalized by Holland et al. (2008). An implementation of this parameterization into a sea–ice–ocean circulation model has shown significant regional and global impacts, as well as a more realistic representation of present-day sea ice cover (Wang and Beckmann 2007). However, due to the simplicity of the ISM parameterization and the coarseness of our model, we do not attempt to predict the ice shelf–ocean interaction quantitatively. Instead, we want to understand the SO processes that would lead global warming to affect the ice shelves. Within this scope, we apply the parameterization to investigate the role of subsurface freshwater and heat fluxes from ISM itself.

## 2 Model description and experiments

### 2.1 The global coupled climate model CLIMBER-3α

The global coupled climate model CLIMBER-3α (Montoya et al. 2005) combines a three-dimensional ocean general circulation model based on the GFDL MOM-3 code with a statistical–dynamical atmosphere model (Petoukhov et al. 2000) and a dynamic and thermodynamic sea–ice model (Fichefet and Maqueda 1997). The oceanic horizontal resolution is $3.75° \times 3.75°$ with 24 variably spaced vertical levels. In addition to a constant isopycnal diffusivity of 1,000 m$^2$ s$^{-1}$, mixing of tracers along surfaces of constant density due to subgrid-scale eddies is parameterized following Gent and McWilliams (1990) with a constant thickness diffusivity of 250 m$^2$ s$^{-1}$. We use an improved version of the model, comprising a deeper Indonesian throughflow and apply a background value of vertical diffusivity of $0.3 \times 10^{-4}$ m$^2$ s$^{-1}$ (Schewe and Levermann 2009). Thus the mixing induced upwelling in both the Atlantic and Pacific ocean in this model is very small (Mignot et al. 2006). In order to focus on baroclinic effects due to the meltwater inflow, wind stress onto the ocean is prescribed using a present-day climatology (Trenberth et al. 1989).

The model has been compared to data for preindustrial (Montoya et al. 2005) and glacial (Montoya and Levermann 2008) boundary conditions. Sensitivity experiments have

been carried out with respect to North Atlantic surface freshwater forcing (Levermann and Griesel 2004; Levermann et al. 2005), global warming (Levermann et al. 2007a) and the reduction in SO winds (Levermann et al. 2007b; Schewe and Levermann 2009).

## 2.2 Basal melting parameterization

Fluxes directly at the ice shelf–ocean interface are discussed by Holland and Jenkins (1999). They are essentially dependent on the local oceanic mixed layer temperature along the base of the ice shelf.

Following Beckmann and Goosse (2003), heat loss and corresponding fresh water flux due to ISM are introduced along the six major Antarctic shelf ice regions in CLIM-BER-3α (Fig. 1). The main assumption in this approach is, that for each ice shelf the average oceanic mixed layer temperature along the ice–ocean boundary is reduced by a constant factor compared to the mean temperature outside the ice shelf cavity. The approach is motivated by partial recirculation and the associated cooling of the ice shelf water within the cavity. The net heat flux $H$ is assumed to be proportional to the temperature difference between the ocean outside the ice shelf cavity ($T_o$) and the pressure melting point at the ice shelf edge ($T_f$). An effective melt area is introduced as tuning parameter to obtain realistic heat fluxes. It is given by the along-shelf width $\Delta l$ in the model geometry and an effective cross-shelf length $L$ (penetration length). Hence,

$$H = \rho_w c_p \gamma L \int_0^{\Delta l} \mathrm{d}l \left(T_o - T_f\right), \tag{1}$$

where $\gamma = 10^{-4} \ \mathrm{m \ s^{-1}}$ is the constant thermal exchange velocity, $\rho_w = 1{,}000 \ \mathrm{kg \ m^{-3}}$ is the reference density of water and $c_p = 4{,}000 \ \mathrm{J(kg \ {}^\circ C)^{-1}}$ is the specific heat of water.

For $T_o$, we choose the temperature at the southern boundary of the model at a constant depth interval between 200 and 600 m along the inferred ice shelf area. This corresponds to the approach of Beckmann and Goosse (2003) and is a fair representation of the entrance of an ice shelf cavity in a coarse resolution model. The salinity dependent pressure melting point is determined in the same area at 200 m depth.

Comparisons with high resolution models that resolve the sub-shelf cavity circulation reveal a relatively uniform penetration length on the order of a few kilometers under various conditions (two and three equation melting formulations) and different cavity geometries (Beckmann and Goosse 2003). This implies, that for a first order approximation, the net melting can be parameterized by shelf ice edge processes, even though a significant portion of the
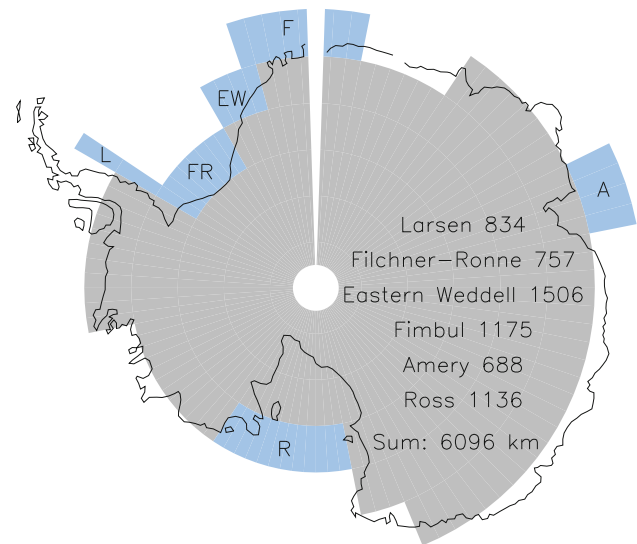


**Fig. 1** Representation of individual ice shelves (*blue*) in CLIM*BER*-3α geometry, framing the ocean model boundary (*gray*). Length of coastline in the model covered by ice shelves (*white space* due to staggered grid). Ocean mean temperatures are diagnosed between 200 and 600 m depth and compared with the freezing point of sea water at 200 m depth. Sub-surface heat and fresh water fluxes are injected at the same place

melting occurs near or at the grounding line. Following Wang and Beckmann (2007), we choose $L = 10$ km to obtain realistic heat fluxes.

Note that the penetration length is not intended to describe the spatial distribution of melt along the ice–ocean interface. It rather determines an effective melt area by reducing the across shelf length to a universal constant. In combination with the temperature difference at the entrance of the cavity, this area represents the size of an ice–ocean interface, which yields heat fluxes corresponding to the integrated melting obtained by a spatially varying heat exchange at the real ice–ocean boundary.

Through latent heat $L_i = 3.34 \times 10^5 \ \mathrm{J \ kg^{-1}}$ and the density of ice $\rho_i = 920 \ \mathrm{kg \ m^{-3}}$, the heat flux is directly converted into fresh water flux into the ocean $F = H/(\rho_i L_i)$. For each shelf, the fresh water flux is converted into annual mean melt rates, using values for the shelf surface area as calculated by Giovinetto and Bentley (1985).

Extending the linear approach by Beckmann and Goosse (2003) and Holland et al. (2008) find a non-linear response of ISM to warmer waters offshore from the ice front. By using a high resolution model and scale analysis, they propose the general applicability of a simplified quadratic relationship between ocean temperature and ISM.

Here we introduce a varying exponent α in order to investigate the effect of different parameterizations. The constants in Eq. 1 are chosen to produce realistic melt rates in preindustrial equilibrium. From this, we derive a proper formulation for the non-linear approach, which matches the

linear case in equilibrium. The heat flux is thus computed as

$$H = \rho_w c_p \gamma L \int_0^{\Delta l} \mathrm{d}l \, \Delta T_{\mathrm{equ}} \left( \frac{T_o - T_f}{\Delta T_{\mathrm{equ}}} \right)^{\alpha}, \qquad (2)$$

where $\Delta T_{\mathrm{equ}} = (T_o - T_f)_{\mathrm{equ}}$ is the temperature difference for the preindustrial equilibrium simulation and $\alpha \in [1,2]$.

Originally, the results of Holland et al. (2008) are based on a temperature dependent exchange velocity within the mixed layer, which however is set constant in Eq. 2. Considering the above mentioned interpretation of $L$, $\gamma$ also becomes a universal scaling parameter rather than a physical quantity of an individual ice shelf.

### 2.3 Global warming experiments

Simulations presented here start from a multi millennia integration (approx. 15,000 years) with preindustrial boundary conditions of 280 ppm $CO_2$ equivalent GHG concentration. In addition to a preindustrial state without ISM, we generate an equilibrium with the ISM parameterization applied according to Eq. 1 during the last 2000 years of the simulation. This simulation is used to determine the equilibrium temperature difference, $\Delta T_{\mathrm{equ}}$ in Eq. 2, for the approach with a non-linear response of ISM to varying ocean temperature in the warming scenario.

Based on these equilibria, we run a scenario with a 1% per year increase of $CO_2$ until quadrupling after approx. 140 years, after which it is kept constant at $4 \times 280$ ppm = 1,120 ppm. This increase represents the upper end of the IPCC scenarios and should be compared with the A2 simulations. With this forcing, the model is integrated over a total period of 1,000 model years. In addition to one experiment with no melt fluxes applied (noISM), we couple both the heat and fresh water fluxes with different exponentiation $\alpha = 1$ and 2.0. In this coupled case, the applied basal melt fluxes are calculated according to Eq. 2 for each time step. In order to investigate the respective influence of the fluxes separately, two supplementary experiments were realized, where either the heat (fixH) or the freshwater flux (fixF) is prescribed according to the equilibrium state. For comparison of the different experiments, annual mean melt fluxes are always diagnosed from the in situ temperature and salinity field. Experiments are summarized in Table 1.

### 2.4 Representation of the Southern Ocean circulation

There are several limitations in the applied climate model, which should be kept in mind while considering our results.

In this study we focus on large-scale circulations in the SO. The performance of a realistic representation of these features varies widely among present coarse resolution

**Table 1** Experiments with different basal melt fluxes to the ocean

| Exp. name | $\alpha$ in Eq. 2 | $H$ to ocean | $F$ to ocean |
|---|---|---|---|
| noISM | 1 | None | None |
| $\alpha = x$ | $x$ | Coupled | Coupled |
| fixH | 1 | Equ. rate | Coupled |
| fixF | 1 | Coupled | Equ. rate |

In all experiments, hypothetical melt fluxes are diagnosed according to Eq. 2 from the in situ temperature and salinity field

models. The strength of the ACC is strongly dependent on realistic topography and the proper representation of baroclinicity due to forcing and internal mixing (Olbers et al. 2006). With preindustrial equilibrium conditions, CLIM*BER*-3$\alpha$ simulates the ACC with a volume transport of approximately 71 Sv ($71 \times 10^6$ $m^3$) through the Drake Passage, whereas observations indicate a total annual mean transport of $134 \pm 11.2$ Sv (Cunningham et al. 2003). Topography is only poorly represented due to the model's coarse resolution. Also eddy diffusive mixing processes, which are probably important in the ACC, are only parameterized. Moreover, coarse resolution models generally tend to blur density gradients, which may cause a weaker current.

Nevertheless, our simulations show an Ekman pumping induced geostrophic balance of baroclinic and barotropic pressure gradients to be the main contributor to the ACC. Hence, we claim to capture the main dynamics of the current, which will show a qualitatively similar behavior within a stronger and more realistic ACC.

Furthermore, we discuss the varying SPG strength and its implications for southward advection of heat. Observations of SPG transport are generally sparse. However, the simulated gyre strength of approximately 28 Sv for the Ross and 46 Sv for the Weddell Gyre are close to the values referred to in the model intercomparison of Wang and Meredith (2008), assuming the barotropic component of the Ross Gyre (which has not been measured yet) to contribute to the overall transport with a similar fraction as it is found for the Weddell Gyre. The simulated SPG strength is also comparable to the values given by the 20 IPCC AR4 Coupled Climate Models gfdl_cm2_0 and the ukmo_hadgem1 referred to in the same study. Similar to the Northern Hemisphere Gyre (Born and Levermann 2009), Wang and Meredith (2008) emphasize the importance of the baroclinic structure of the SPGs, whereas they find only a weak link between gyre strength and wind curl. We analyze the varying SPG strength due to density changes. With the same limitations as for the ACC, our results will also be valid for a more realistic representation of the SPGs, mainly depending on the quality of the parameterized mixing processes.

Another strong limitation of our model is the fixed wind stress on the ocean, which is prescribed by a present day climatology throughout the entire simulation. Despite the direct acceleration of large scale currents, wind stress is an important energy source for upwelling in the SO. It sets up the meridional density structure of the ACC and the SPGs and causes warm deep water to enter the ice shelf cavities. Thus varying wind stress needs to be considered for a proper projection of SO circulation under global warming. Nevertheless, our simulations allow clear identification of the main mechanisms based on density changes, which may be superimposed onto the effects of varying winds.

## 2.5 Validity of the ISM parameterization

In this study, we scale ISM in comparison to cavity-resolving models to produce realistic melt rates for the equilibrium simulation. To capture the sensitivity of ISM to oceanic changes, we apply a generalized dependency on bulk ocean properties. This is consistent within the frame of the coarse resolution model, which is designed to qualitatively analyze the interaction of a broad range of different processes within the climate system. Nevertheless, this parameterization is a poor representation of the net effect of the sub-shelf circulation, which depends strongly on cavity shape, the effects of on-shelf sea–ice growth (Nicholls 1997), shelf-break upwelling and tides. These effects are not captured by our model and may significantly alter the response of ISM to global warming.

Our model only parameterizes melt along the six largest ice shelves around the Antarctic continent. Especially the ice shelves in the Amundsen Sea and Bellinghausen Sea, which are currently suspected to produce high melt rates in response to climate change, are neglected (Rignot et al. 2008). Considering the resolution of the oceanic component in CLIMBER-3α, these ice shelves are clearly on a subgrid-scale and their cavity entrance would not be properly represented in the model. Also the suggested scaling by use of a general penetration length was only done for larger ice shelves with different proportions in previous studies. When trying to include them we obtained very small melt rates due to their relatively small width.

Finally ice shelf cavities are evolving due to melt and freezing, as well as internal ice dynamics. All associated effects on ISM are neglected. This is partly justified because regional high resolution model studies reproduce realistic conditions and simulate the evolution of an ice shelf–ocean system with dominant melt rates at the shelf edge and at the grounding line (Grosfeld and Sandhäger 2004; Williams et al. 2001). From those studies, we expect low sensitivity of the penetration length to changes in the shelf geometry, especially the decreasing distance from the grounding line to the shelf edge.

However, the assumption of a static ice shelf in a warming climate is unlikely to produce realistic melt rates.If the warming signal is strong enough, shrinkage of the ice–ocean interface is likely to occur in all areas of non-marine ice sheets. Our approximation thus probably increasingly overestimates the response of ISM during the simulation.

Nevertheless, Walker and Holland (2007) show that the adjustment of ice shelves to perturbations in ocean temperature are on the order of several decades up to a few centuries, which is much slower than the adjustment of the circulation. Therefore, we may capture a realistic sensitivity of melt rates associated with increasing oceanic temperatures, given by our model at the beginning of the simulation.

To account for the deficiencies of the ISM parameterization, the analysis in this study will be done on two timescales: (1) in order to investigate the evolution of the SO circulation under global warming and subsequent implications for ISM, we regard the whole simulation length; and (2) while analyzing the parameterized response of ISM and its effect on ocean dynamics, we focus on the first 200 years of the simulation, because we cannot trust the assumption of static ice shelves on longer timescales.

## 3 Response of SO circulation to global warming

Rising atmospheric and oceanic temperatures due to global warming affect the horizontal SO circulation in CLIMBER-3α (Fig. 2). First, we analyze the geostrophic component of the ACC and the SPGs without considering the influence of ISM. In Sect. 5, we additionally consider the effect of ISM on the circulation.

### 3.1 Geostrophic contribution to ACC

In the SO, the meridional density gradient between cold dense water in the south (shallow pycnocline) and lighter warm water in the north of the SO balances the ACC in preindustrial equilibrium. The interjacent current comprises an area of outcropping isopycnals (Fig. 3a).

Integrating the geostrophic balance for a two-dimensional cross-section from south ($y = S$) to north ($y = N$) and from depth ($z = H$) to sea surface ($z = \eta$), the zonal volume transport is given by

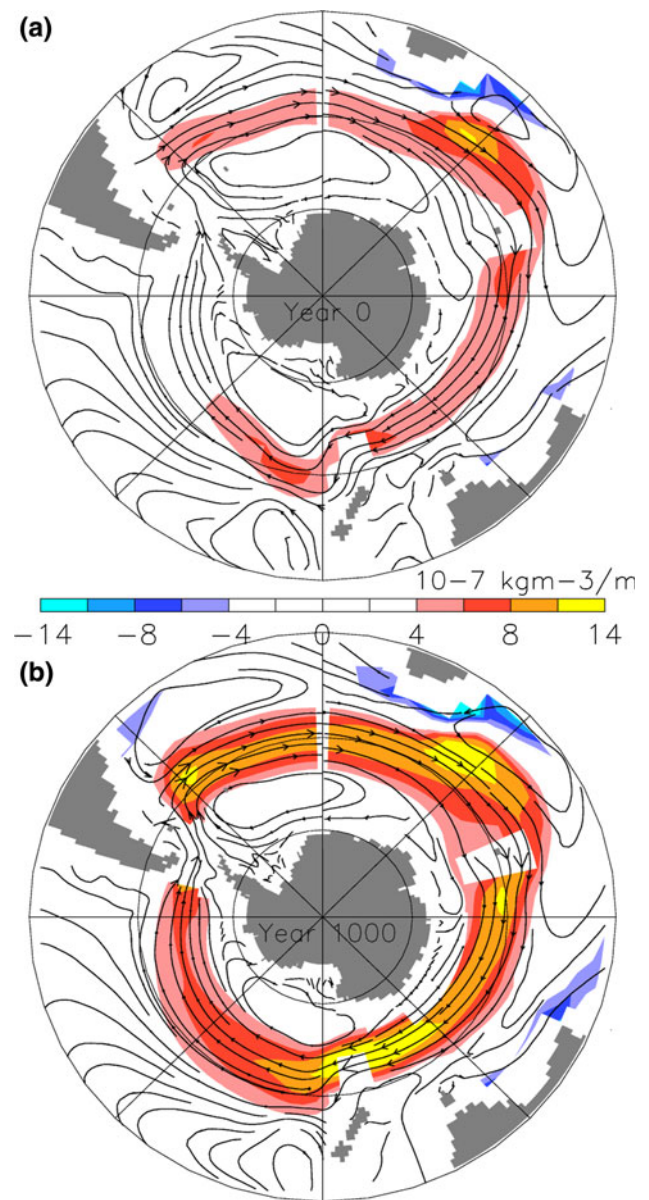$$M = \int_S^N \mathrm{d}y \int_H^\eta \mathrm{d}z \cdot u = \int_S^N \mathrm{d}y \int_H^\eta \mathrm{d}z \frac{-1}{f \rho_0} \frac{\partial p}{\partial y}, \qquad (3)$$

where $u$ is the zonal velocity, $p$ is the pressure, $f$ the Coriolis parameter and $\rho_0 = 1{,}035$ kg m$^{-3}$ the reference density of seawater.
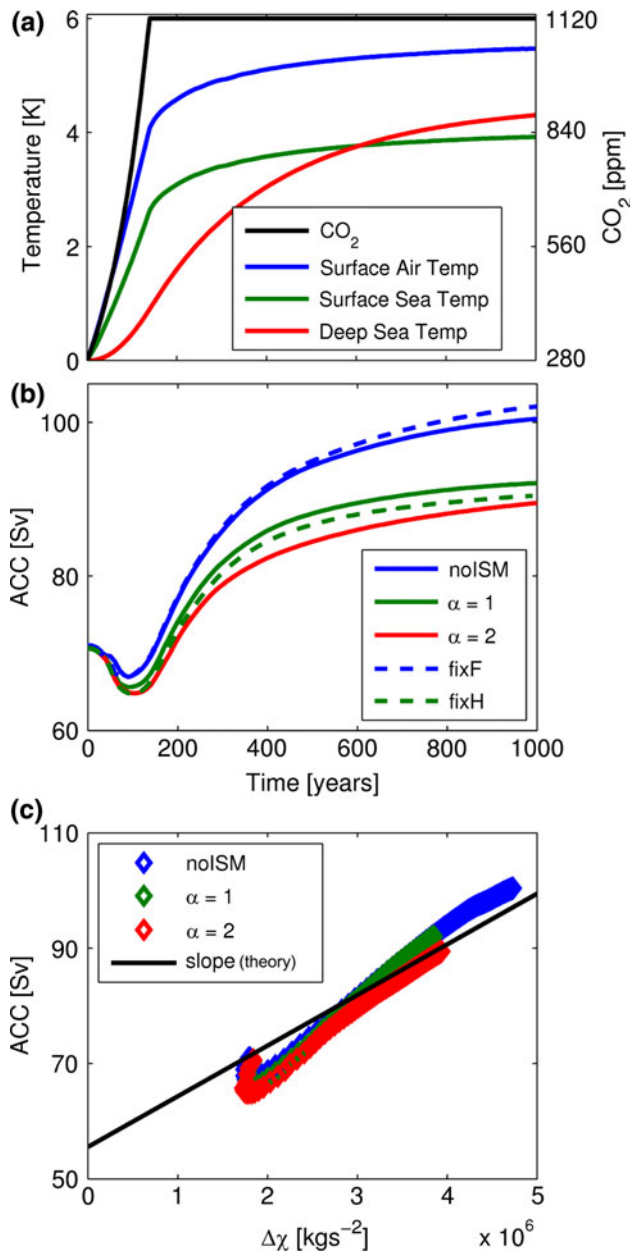
**Fig. 2 a** Timeseries of atmospheric $CO_2$ and anomalies of global mean surface air temperature, global mean sea surface temperature and global mean deep ocean temperature from 500 to 2,000 m depth for the noISM run. **b** Timeseries of maximum transport of Antarctic circumpolar current (*ACC*) for different experiments. **c** Correlation between ACC transport and potential energy difference across the ACC averaged to 2,000 m depth for different experiments, as well as linear fit (*black line*) with the slope, given in Eq. 6

**Fig. 3** Horizontal velocity streamlines (*black lines*) averaged down to 2,000 m depth. The meridional derivative of potential density (*colors*) at 800 m depth south of 30°S shows the regions of strongest outcropping. The slope of isopycnals in the ACC increases under global warming in noISM. **a** Beginning of the simulation, **b** after 1,000 years

Assuming the Boussinesque approximation and a constant Coriolis parameter ($f_0 = -1.1 \times 10^{-4}$ s$^{-1}$), the pressure term can be split into a sea surface elevation and a baroclinic component. The zonal volume transport then becomes

$$M = \frac{-g}{\rho_0 f_0} \int\limits_S^N \mathrm{d}y \left[ \int\limits_H^0 \mathrm{d}z \left( \eta \rho_0 + \int\limits_z^0 \mathrm{d}z' \rho(z') \right) \right]. \quad (4)$$

Assuming a level of no motion, $z = -L$, at which the barotropic pressure force in $y$-direction is balanced by its baroclinic counterpart, we can replace the sea surface elevation term to obtain

$$M = \frac{g}{\rho_0 f} \left[ L \int_{-L}^{0} dz \rho(z) - \int_{-L}^{0} dz \int_{z}^{0} dz' \rho(z') \right]_{S}^{N}. \quad (5)$$

The term in square brackets equals (baroclinic) potential energy (partial integration). Thus we expect the ACC strength to correlate linearly with the meridional difference of potential energy ($\Delta\chi$) across the ACC:

$$M = \frac{1}{\rho_0 f} \Delta\chi = \frac{g}{\rho_0 f} \left[ \int_{-L}^{0} dz \rho(z) z \right]_{S}^{N} \quad (6)$$

Figure 2c shows that volume transport through the Drake Passage correlates well ($r = 0.99$) with the potential energy difference down to 2,000 m depth between two zonal rings north and south of the current. The diagnostic areas for $\Delta\chi$ are indicated in Fig. 6a. The slope ($a = 8.8 \ m^3 \ s(kg)^{-1}$) of the line is given by the constants in Eq. 6. For a solely geostrophic and zonally homogeneous current, the line would meet the origin. The analyzed density distribution here is heterogeneous across the SO and very sensitive to the diagnostic area. The zonal ring in the north does not entirely cover the extent of the current. Therefore, the approximation of a bulk density that accounts for the energy budget of the ACC is difficult to fulfill. Note that according to Eq. 6, the significance of density differences increases with depth.

In addition to the geostrophic component, direct acceleration due to wind stress is an important energy source. Atmospheric winds are prescribed during the simulation and the effect of varying oceanic surface stress due to decreasing sea ice cover is found to be small. Hence the wind stress component is relatively constant and does not cause the observed changes in ACC strength.

## 3.2 Temporal evolution of the density field

To investigate the changes of the ACC under global warming, we decompose the changes in potential energy into respective contributions caused by salinity and temperature. We analyze the noISM experiment and compute the timeseries of the density field by only taking changes either in temperature or salinity into account. The respective other field is kept in the equilibrium state for the whole timeseries (Fig. 4a).

Under global warming, two competing effects determine the density gradient across the current. Initially, the warming leads to decreasing sea ice cover around Antarctica, which reduces northward sea ice export (contours Fig. 4b). This causes a strong freshening in the south that weakens the meridional density gradient and decelerates
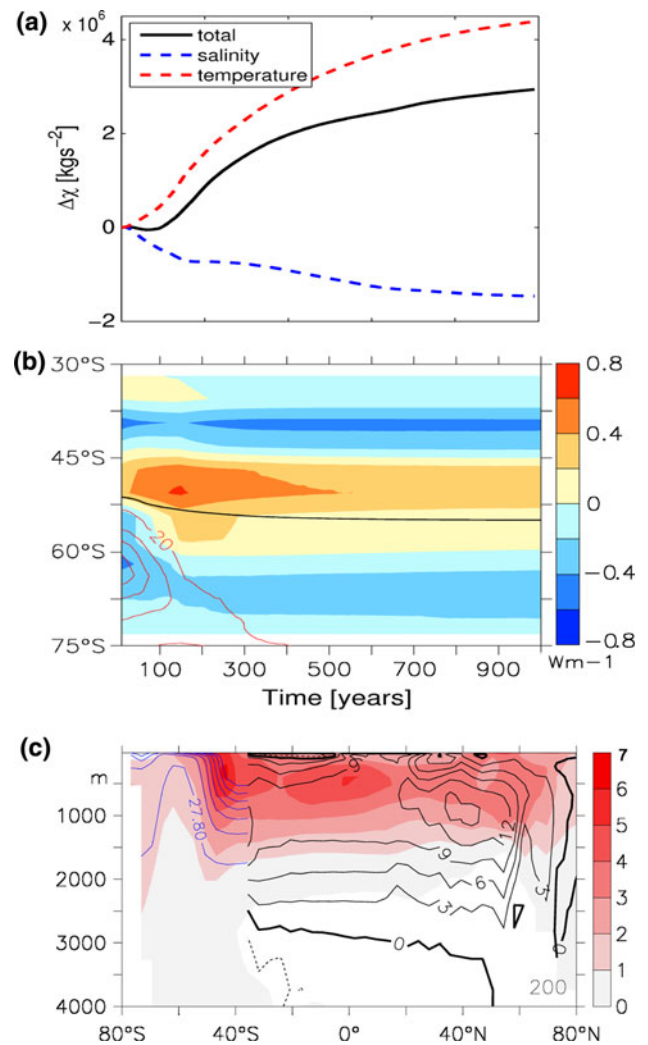


Fig. 4 a Timeseries (noISM) of zonal mean potential energy difference across the ACC averaged over upper 2,000 m depth for no ISM. *Dashed lines* indicate the contribution from salinity changes and temperature changes, respectively. A strong freshening in the south initially slightly weakens the ACC. After 100 years, the northerly warming enhances the difference in potential energy. b Hofmueller diagram of zonal mean ocean heat flux. The *black line* indicates the zonally averaged latitude of maximum ACC strength. *Contours* indicate annual and zonal mean northward sea ice export (mSv). Ocean heat uptake is strongest north of the ACC and expands southward as the sea ice is melting. c Atlantic temperature anomaly after 200 years over Atlantic overturning circulation (Sv, *black contours*) and SO isopycnals between 40°W and 20°W (*blue contours*)

the ACC. The effect saturates after about 150 years, when most of the sea ice has vanished. Furthermore, precipitation increases at high latitudes and decreases the density gradient (not shown).

The dominating long term effect is a strong warming along the northern boundary of the current (Fig. 4c), which yields to steepening isopycnals in the outcropping regions

(Fig. 3). Consequently, the volume transport through the Drake Passage increases from 71 Sv initially to 102 Sv after 1,000 model years.

### 3.3 Warming response of the Ross and Weddell Gyre

Similar to the North Atlantic Subpolar Gyre (Myers et al. 1996; Levermann and Born 2007), geostrophic currents around centers of dense water contribute to the large cyclonic eddies in the Ross and Weddell sea. The northern boundaries of the SPGs merge with the ACC. In the south, the approximately 2,000 m deep currents are limited by the continental shelf break.

Similar to the ACC, we observe variations of SPG strength due to changes in baroclinicity. In the region between 150°W and 180°W in the Ross and 10°W and 30°W in the Weddell sea, we diagnose maximum zonal transport through a meridional cross-section south of the center of the SPGs. The center of the Ross gyre (approx. 66°S in our simulations) is located further south than the Weddell Gyre (approx. 61°S in our simulations). The temporal evolution of the currents under global warming is shown in Fig. 5. As with the ACC, the meridional difference in potential energy is diagnosed in the same area as the transport and correlates well ($r = 0.93$) with SPG strength.

In the noISM simulation, a combination of the sea–ice effect mentioned in Sect. 2, increasing precipitation in high latitudes (Manabe and Stouffer 1980) and the warming



**Fig. 5** Timeseries of **a** Weddell Gyre and **b** Ross Gyre transport for different experiments. ISM increases gyre strength under global warming

signal from the north determine the slope of isopycnals across the SPGs. A strong surface freshening close to the Antarctic coast initially increases the density gradient and predominantly strengthens the current during the first 300 years of the simulation.

After the surface fluxes have stabilized, SPG strength is determined by warming of the northern boundary and a freshening signal which penetrates the center of the gyres at depth. This signal originates from the north Atlanic. In agreement with previous studies (Rahmstorf and Ganopolski 1999), we find a freshening of the Nordic Seas due to increased precipitation at high latitudes. This signal is spread within the deep ocean convection (lower branch of NADW) and reaches the center of the SPGs by isopycnal diffusion after several centuries. Finally, the current strength stabilizes on a significantly higher level compared to the equilibrium state.

## 4 Oceanic heat uptake and transport to ice shelves

Although atmospheric warming is strongest in the polar regions, it does not access the ice shelves directly through the adjacent ocean surface. Temperature anomalies are rather convected and transported southward by the deep ocean. Varying ACC strength as well as the advection within the SPGs are crucial for the meridional heat transport. The additional effect of ISM on the changing circulation is not considered but is discussed in Sect. 2.

### 4.1 Heat uptake and deep ocean warming

Under conditions of increased $CO_2$, most additional heat penetrates the ocean in the northern and southern outcropping regions (Fig. 4b). Especially in the ACC, we observe high temperature anomalies down to 2,000 m throughout the entire simulation (Fig. 4c).
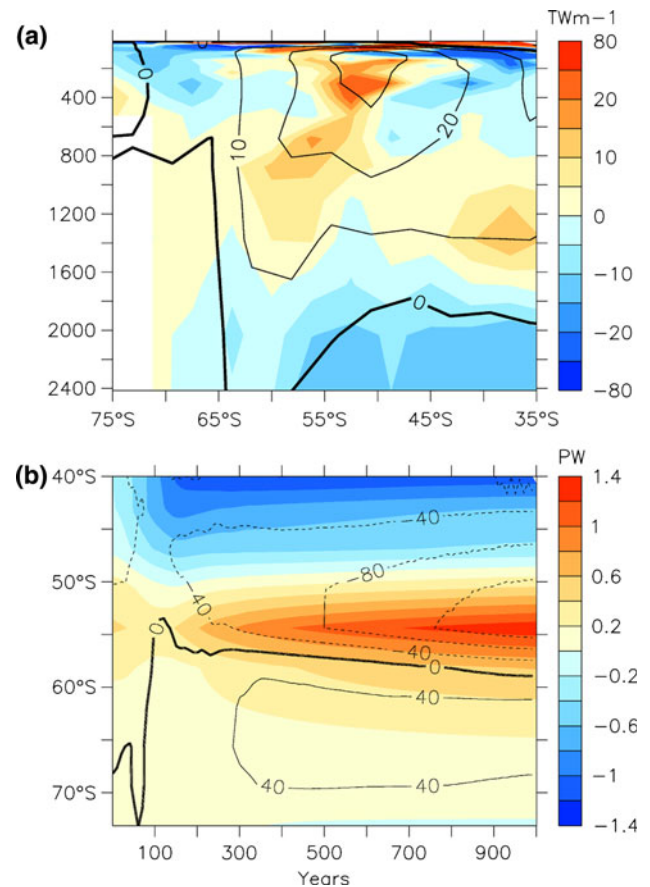
The dominant cause of deep ocean warming is mixing along surfaces of constant density. In the outcropping regions, isopycnal mixing connects surface water with the deep ocean and is much more efficient than diapycnal mixing (Toole et al. 1994). Hence the warming signal propagates faster downwards compared to regions with strong stratification.

The warming at depth is distributed around Antarctica following the ACC and SPGs (Fig. 6). Advection within the SPGs transports warm water across latitudes and mixes CDW from the ACC towards the coast and the ice shelf areas (Fig. 7a). Close to the coast, highest temperature anomalies occur between 200 and 2,000 m depth. Especially in the Weddell Sea, warming is strongest where deep water flows towards the continental-shelf. The meridional overturning within the Deacon-cell (here defined as
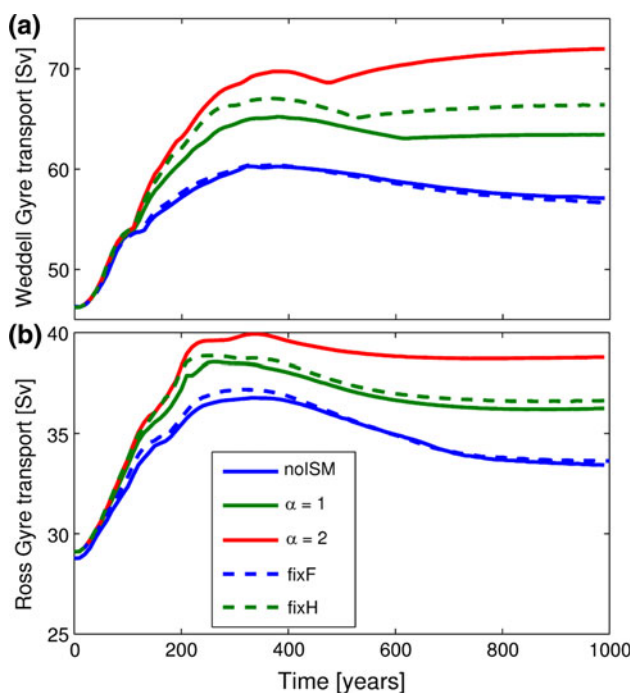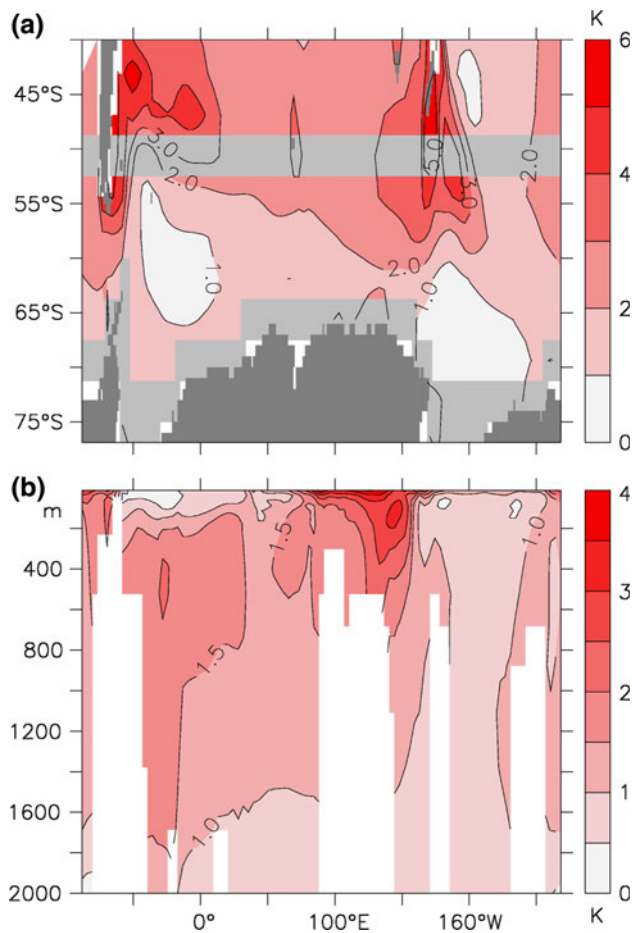
**Fig. 6 a** Mean temperature anomaly in the SO averaged to 2,000 m depth after 200 years in the noISM run. **b** Cross-section of meridional mean temperature anomaly after 200 years in the *gray shaded* area in **a** framing the Antarctic continent. SO warming is strongest below the surface and coincides with large-scale advection pattern. *Gray shaded* areas in **a** also indicate areas where potential energy is determined in Sect. 3



**Fig. 7 a** Zonal mean southward heat transport anomaly from advection and eddy diffusion after 1,000 years (noISM). *Contours* indicate the Deacon cell (Sv). Advection warms the SO below the surface. **b** Hofmueller diagram of southward advective heat transport in the noISM run (*colors*) and additional anomaly due to ISM with α = 1 (TW, *contours*). The total southward advection of heat is well correlated with ACC strength. ISM causes additional heat transport in the enhanced SPGs

vertical–meridional streamfunction Ψ in the SO) does not increase significantly in strength but at 1,000 m depth it is shifted towards a greater meridional extent. The slowest warming occurs at the center of the SPGs. Here, advection is weak and horizontal diffusion is limited by outcropping isopycnals (Fig. 4c).

### 4.2 Southward advection of heat

Next we identify the dominant mechanism that distributes the warming signal in the SO. We decompose the meridional heat transport into three different components. (1) Zonal integration of the product of temperature and meridional velocity from the surface to the sea bed gives the advective component. (2) Analogous, the contribution of eddy diffusion is obtained by replacing the meridional velocity with the parameterized effective eddy transport

velocity (Gent and McWilliams 1990). (3) Isopycnal diffusion is also parameterized but difficult to reproduce from the model output. Instead we infer it from the ocean net heat budget for preindustrial equilibrium, which should be zero, taking the surface flux into account. Note that in our model only resolved advection (1) causes volume transport, whereas parameterized mixing (2) and (3) only propagates ocean tracers.

With 0.24 PW ($0.24 \times 10^{15}$ W), advection provides the largest southward heat transport between 50°S and 60°S, while eddy diffusion contributes with 0.14 PW, in equilibrium. The annual mean surface heat loss accounts for 0.45 PW, thus isopycnal diffusion should contribute with 0.07 PW. Hence, the net heat transport is relatively equally distributed between resolved advection and parameterized mixing.

By analyzing the temporal evolution of the different components, we determine the main contributor to SO

warming. The southward heat transport by eddy diffusion rises with global warming due to an increased meridional temperature gradient, but it does not exceed 0.5 PW. Southward isopycnal diffusion cannot be computed, but generally plays a minor role in the ACC, where it rather transports heat to depth or northwards, following the outcropping isopycnals.

However, the meridional advection of heat increases drastically up to 1.3 PW by the end of noISM (Fig. 7b). Even if isopycnal diffusion would increase at a similar high rate, the advective component would greatly exceed the overall contribution from mixing. Moreover, the advective heat transport is well correlated ($r = 0.98$) with zonal volume transport through Drake passage, i.e. ACC strength. Hence we conclude that the acceleration of the ACC is crucial for ocean warming south of 60°S.

Although the distinction between advection and diffusion is entirely a function of the coarse grid resolution, it allows us to link the meridional heat transport directly to the resolved large-scale flow. The meridional component of the ACC continuously advects across latitudes. Thereby, mixing reduces temperature gradients as warm water from the northern regions with high oceanic heat uptake reaches colder areas in the south and vice versa. Note that the role of mixing in this process is different, compared to a purely diffusive meridional transport of heat. It does not act in a certain direction but rather mixes water masses with different properties which were advectively brought together.

Two effects strengthen this process under global warming: (1) the increasing meridional temperature gradient across the current enhances local mixing; and (2) the accelerated current itself transports more heat across latitudes and towards the mixing areas. The good correlation between the (even partly decreasing) ACC strength and the diagnosed meridional heat transport indicates that increasing volume transport is more important than the rising temperature gradient.

In Sect. 2, we have shown that the strengthening of the ACC and the SPGs is caused by the deep ocean warming north of the currents. Therefore, the increased SO heat uptake enhances warming close to the Antarctic coast (and associated ISM) in two ways. On the one hand, meridional mixing of heat is directly enhanced by larger temperature gradients. On the other hand, advection of heat is enhanced within the accelerated large-scale circulation.

## 5 Meltrates in equilibrium and under global warming

Parameterized ISM in equilibrium reproduces results from earlier studies. Under global warming, melt rates increase drastically. Local cooling due to ISM limits the increase. The applied freshwater flux affects the response of SO circulation to global warming.

### 5.1 Evolution of ISM and coupling effects

Heat and freshwater fluxes, as well as melt rates, for the coupled preindustrial equilibrium are shown in Table 2. The values are comparable to those found by Beckmann and Goosse (2003), which applied ECMWF and NCEP climatologies to force a cavity resolving regional ocean circulation model. Comparison with another study of Hellmer (2004), which also simulates ice shelf cavities within a regional high resolution ocean circulation model shows similar melt rates, as given in Table 2. The discrepancy between freshwater fluxes and melt rates for the Amery and the Eastern-Weddell ice shelves is due to different ice shelf areas used for computation in the study of Hellmer (2004). The total applied fresh water fluxes of all different studies are between 28 and 30 mSv. Without coupling, the values are generally higher due to the absence of local ISM cooling.

Only at the Amery ice shelf (AIS) is our ISM one order of magnitude higher than predicted by Hellmer (2004). This is most likely an overestimate due to the poorly resolved topography, since the ice shelf is not protected by any continental shelf in our model geometry. However,

**Table 2** Induced ice shelf areas characterized by their surface area, calculated by Giovinetto and Bentley (1985)

| Ice shelf | Area ($10^5$ km$^2$) | $\Delta T$ (K) | $F$ (mSv) | Meltrate (m a$^{-1}$) | Year 200 factor |
|-----------|----------------------|----------------|-----------|-----------------------|-----------------|
| Amery     | 0.75                 | 0.77           | 6.8 (0.6) | 2.9 (0.4)             | 3.1             |
| E-Weddell | 0.82                 | 0.28           | 5.6 (5.2) | 2.2 (2.4)             | 5.7             |
| Filchner-R| 5.48                 | 0.09           | 1.0 (3.7) | 0.1 (0.3)             | 7.2             |
| Fimbul    | 0.58                 | 0.58           | 8.9 (7.8) | 4.9 (4.9)             | 3.7             |
| Larsen    | 0.66                 | 0.29           | 3.1 (1.2) | 1.4 (0.7)             | 3.1             |
| Ross      | 4.01                 | 0.30           | 4.2 (5.6) | 0.4 (0.5)             | 1.9             |
| Total     | 12.30                | –              | 29.7 (24.1)| –                    | 3.7             |

Simulated difference between ocean temperature between 200 and 600 m depth and pressure melting point at 200 m ($\Delta T$) for the coupled equilibrium run. Associated freshwater flux and spatial average melt rate for the equilibrium run in comparison to the results of Hellmer (2004) (in parentheses). Factor of ISM increase after 200 years of global warming in the $\alpha = 1$ experiment

changes in the SO circulation presented in this study are mainly caused by varying ISM in the Ross and Weddell Sea. Therefore, the mismatch at the remote AIS will probably not influence our results qualitatively.

Changes in hydrology due to ISM compare well with previous studies (Wang and Beckmann 2007; Hellmer 2004; Beckmann and Goosse 2003). Cooling and freshening occurs close to the ice shelf areas. Moreover, the freshening enhances stratification, which reduces vertical mixing. Consequently, large parts of the SO below 500 m are warmer and more saline compared to the control experiment. Colder surface waters between 65°S and 60°S lead to increased sea ice concentration and less heat loss during winter.

The large-scale circulations which undergo significant changes under global warming remain nearly unchanged in the equilibrium when ISM is included. These include the ACC, SPGs, AABW, AMOC and the North Atlantic Subpolar Gyre.

Under global warming, ISM is determined by rising temperatures in the deep SO (Fig. 8). Section 4 illustrates how additional heat is transported towards the ice shelves.

The warming signal at depth continues several centuries after $CO_2$ and global mean temperature have stabilized (Fig. 2a). After the first 200 years, the ocean south of 62°S has warmed about 0.74 K for the noISM and 0.85 K for the $\alpha = 2$ experiment (Fig. 8a). After 1,000 years, we find temperature anomalies between 1.95 K for the noISM and 2.98 K for the $\alpha = 2$ experiment. At the end of the simulation, no equilibrium state was reached.

After 200 years, the initial temperature differences at each shelf ($\alpha = 1$) have increased by the factors given in the last column in Table 2. Thus increased $F$, and melt rates may be computed by multiplying the factor with the equilibrium values. The obtained total basal meltwater rate of 0.03 Sv initially, increases rapidly and reaches between 0.11 Sv ($\alpha = 1$) and 0.25 Sv ($\alpha = 2$) after 200 years. After four centuries the increase saturates to reach between 0.21 Sv ($\alpha = 1$) and 0.77 Sv ($\alpha = 2$) at the end of the simulation. However, it should be noted that values given here are based on the assumption of a constant ice shelf geometry, which is highly disputable for the entire simulation time (Sect. 5).

### 5.2 Basal melting feedbacks on SO response to warming

In the coupled case, a local negative feedback reduces ISM in comparison to noISM, where melt fluxes are calculated without applying them to the ocean. Cooling of the coastal water is not fully compensated by additional southward mixing of heat. Therefore, the fixF experiment reproduces similar melt rates as noISM, whereas melt rates in the fixH
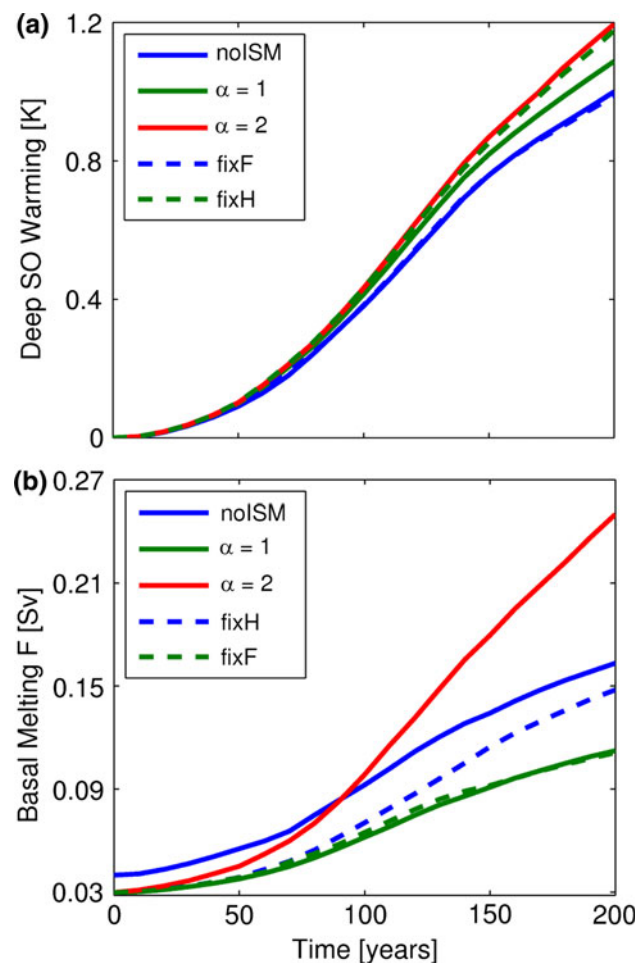


**Fig. 8** Timeseries of **a** SO mean temperature anomaly between 500 and 2,000 m depth south of 62°S for different experiments. **b** Timeseries of total ISM fresh water flux in different experiments. Basal melting increases as the deep ocean temperature increases and enhances heat transport towards the SO

experiment compare well to the $\alpha = 1$ experiment (Fig. 8b). In addition, the heat flux from ISM has no significant influence onto the large-scale ocean dynamics.

The local influence of released freshwater from ISM is relatively weak. Nevertheless, at injection depth it has a measurable impact on the ocean dynamics and hence indirectly alters the heat transport towards the coast (Fig. 9a).

Additional SO warming is caused by stronger gyre circulations due to ISM. ISM-related freshening of the SPG's southern boundaries increases the meridional density gradient and significantly enhances the volume transport of the currents (Fig. 5). The accelerated SPGs enhance southward advection of heat (Fig. 7b). Therefore, the warming south of 65°S and between 500 and 2,000 m is stronger with increasing ISM (Fig. 9b).

A self-amplifying gyre-melting feedback loop may be closed, because enhanced ocean warming causes higher

**(a)**



**(b)**
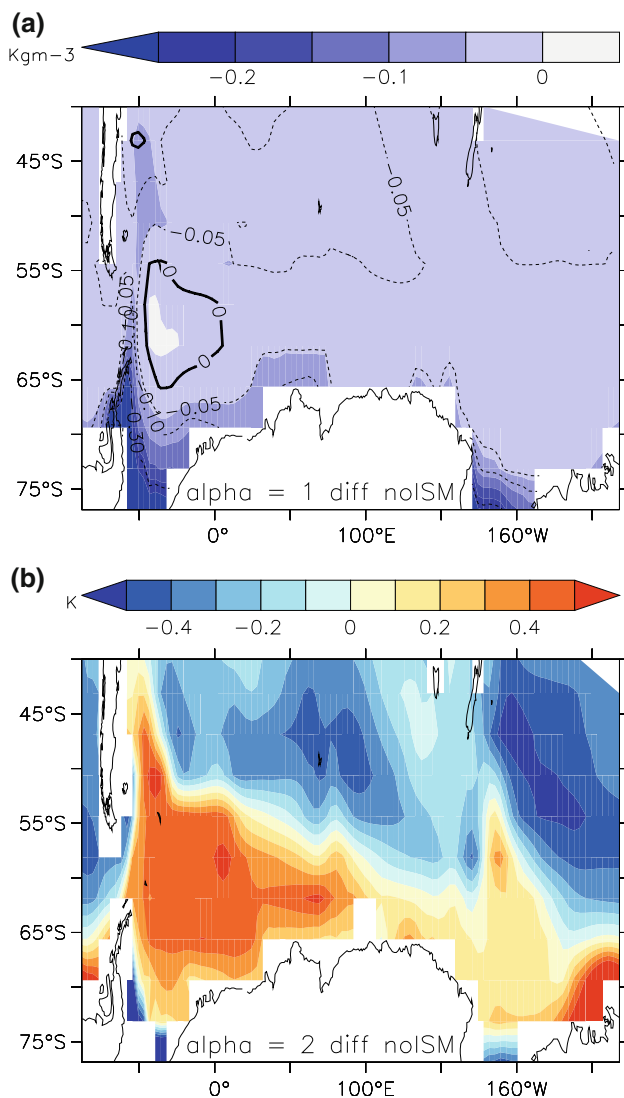


**Fig. 9 a** Mean density difference between $\alpha = 1$ and noISM experiment in the SO down to 1,000 m depth after 200 years. *Contours* indicate the difference in salinity (psu) of the same experiments in the same area. Density anomalies are directly caused by freshening due to ISM. **b** Mean SO temperature difference at 500–1,000 m depth between $\alpha = 2$ and noISM experiment. Increasing ISM causes additional warming of the SO

freshwater flux from ISM, which again accelerates the gyre circulation. However, in our model, this feedback is very weak and does not cause higher melt rates in the coupled simulation compared to noISM. Already in fixH, ISM is for the most part determined by local cooling close to the Antarctic coast. Comparison of the the fixH and fixF experiment with an additional simulation, where ISM is entirely fixed to equilibrium rates, shows that this negative feedback on ISM is about five times larger compared to the above mentioned positive gyre-melting feedback.

Moreover, ISM influences the response of the ACC to global warming. In the coupled case, the current is

generally weaker compared to noISM (Fig. 2b). The potential energy difference across the current is reduced by both the salinity and the temperature field (not shown). On the one hand, ISM causes a direct freshening south of the ACC, which dampens the increase of the current. On the other hand, the increased advection of heat due to the accelerated SPGs reduces the temperature gradient across the current.

Although the weaker ACC reduces the meridional heat transport north of 55°S, deep ocean mean temperature south of the ACC rises with increasing ISM (Fig. 8a). This implies a minor role of the ACC response to ISM compared to the SPG acceleration.

While the NADW is only marginally affected by ISM, the formation of AABW initially diminishes due to the warming and can only recover to a drastically reduced state because of the freshwater flux in the coupled case.

# 6 Conclusion and discussion

## 6.1 Aim of the study

We analyze global warming experiments from the Earth system model of intermediate complexity CLIM*BER*-3$\alpha$ in order to tackle the question of how decadal- to centennial-time-scale atmospheric warming may reach the Antarctic ice shelves. To incorporate possible feedback mechanisms, fluxes from ISM are inferred from an assumption on their dependency on bulk ocean properties. Two major findings are presented in this paper: (1) the strengthening ACC is the largest contributor to additional warming of the SO, leading to enhanced ISM under global warming; and (2) three ISM related feedback loops influencing SO circulation are identified (Fig. 10). Among these, local oceanic cooling dominates and reduces ISM in the coupled case.

## 6.2 Southward advection of heat within the ACC

In agreement with observations (Böning et al. 2008), atmospheric warming penetrates the deep ocean in the southern outcropping regions in our model. The warming causes a steepening of isopycnals and enhances ACC volume transport on centennial timescales. This behavior confirms previous coarse resolution modeling studies (Bi et al. 2002), which found a correlation between ACC strength and density difference across the current.

Warming of the SO and associated ISM is subsequently dominated by varying ACC strength. Advection within the current provides most of the southward oceanic heat transport in our model. The processes causing meridional overturning within the observed ACC are complex (Olbers et al. 2004) and mixing of watermass properties across the
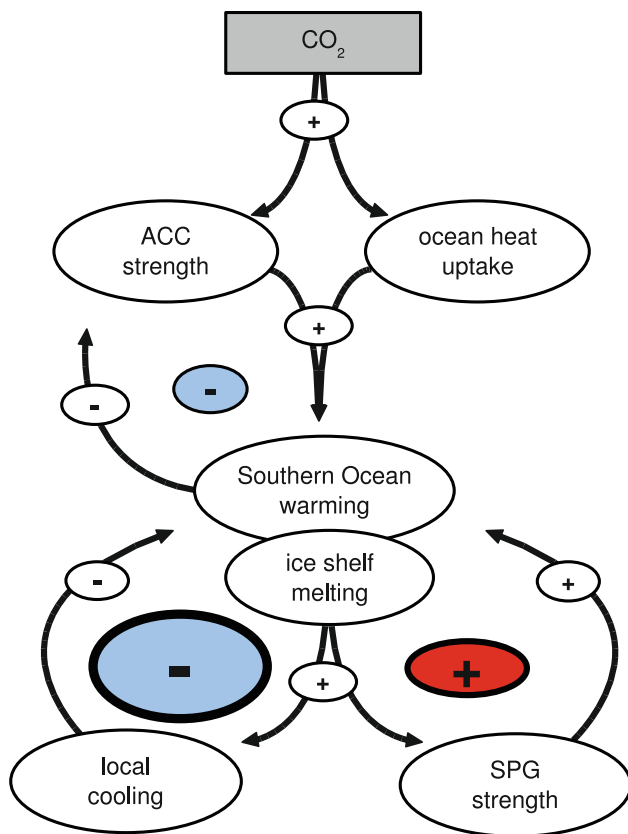
**Fig. 10** Rising atmospheric temperatures ($CO_2$) enhance SO warming and associated ISM in two ways. Isopycnal diffusion transports heat to depth and increases the meridional temperature gradient across the ACC (ocean heat uptake). In addition to increased southward mixing of heat, the accelerated ACC enhances southward advection of heat (ACC strength). Initially, steepening of isopycnals is dampened by less northward export of sea–ice, until its decline saturates (not shown). If basal melt fluxes are coupled to the ocean, ISM will be weaker. Mixing limited local cooling at the shelves forms a dominating negative feedback. Secondarily, the gyres reveal a self-amplifying feedback with ISM. Melted freshwater increases the across gyre density gradient (SPG strength), causing an additional warming of the SO. As a minor negative feedback, ISM also dampens the increase of ACC strength

current is not yet fully understood. We find that heat is transported due to the meandering of the ACC across latitudes and the associated meridional flow from warmer latitudes to the colder south. This effect is enhanced within a stronger ACC.

The validity of these results is restricted by the coarseness of the oceanic resolution within CLIM*BER*-3α. For example, meso-scale eddies, which are expected to be important for the ACC (Garabato et al. 2007; Saenko and Weaver 2003) are only parameterized. A more realistic representation of mixing processes will probably change the distribution of heat transport (Hallberg and Gnanadesikan 2006). However, Olbers et al. (2004) hypothesize that both, the zonal current, as well as diffusive mixing due

to meso-scale eddies are caused by the meridional density gradient across the current. Therefore, we propose that a stronger ACC will be correlated with more meridional heat transport for eddy resolving models, as well.

Moreover, in Sect. 4 we mentioned the weaker volume transport of 71 Sv through the Drake Passage compared to observations (Rintoul and Sokolv 2001). This discrepancy needs to be addressed to obtain a realistic meridional heat transport. However, we believe that the mechanisms described here are qualitatively robust with respect to model improvements, since they depend predominantly on the geostrophic balance. We furthermore hypothesize that the effects of advective mixing will be stronger for a stronger ACC compared to the modelled one.

The decreasing ACC strength during the first century of our simulation has not been observed in previous modeling studies (Fyfe et al. 2007; Fyfe and Saenko 2006; Bi et al. 2002). During this period, a freshening of the southern boundary of the ACC determines the slope of the isopycnals. The combined effect of decreasing northward sea ice export and increasing precipitation in southern high latitudes weakens the ACC strength. This hypothesis is supported by an observed freshening trend at the southern boundary of the current (Böning et al. 2008). Likewise, enhanced precipitation is presently observed (Thomas et al. 2008).

However, the initial increase in ACC strength in other models was probably due to increasing SO winds, which are kept constant in our simulation, in order to see the baroclinic adjustments more clearly. On the other hand, the actual influence of varying wind stress on volume transport within the ACC, as well as on ocean heat uptake, has recently been questioned (Böning et al. 2008), again emphasizing a greater importance of meso-scale eddies. Anyway, the purely barotropic contribution of the winds to the ACC is very weak (about 2 Sv) and any significant wind-induced changes need to comprise a baroclinic response. Further studies are needed to determine which effects are dominant.

### 6.3 Ice shelf melting feedbacks and accuracy of melt rates

Previous modeling studies have suggested large-scale and global influences of ISM sub-surface fluxes on the ocean circulation (Losch 2008; Wang and Beckmann 2007; Hellmer 2004; Beckmann and Goosse 2003). These studies were restricted to (partially regional) diagnostic simulations of the present day climate conditions of rather short integration time. In this study, the effect of ISM was included in a coupled global climate model, which was used to simulate the evolution of the SO circulation under global warming for several centuries. However, this study

is not meant to present a realistic projection under global warming, but rather a sensitivity study emphasizing (and potentially exaggerating) possible baroclinic mechanisms which should be investigated in higher resolution models. We find that freshwater fluxes from ISM increase drastically under global warming. However, the applied ISM parameterization suffers from many deficiencies, as discussed in Sect. 5. It should be regarded as a zero order approximation of the ocean's sensitivity to ISM, as to be consistent with the resolution of the entire oceanic component. Within this framework, we find that ISM significantly influences the large-scale circulation and may alter the heat budget of the SO in several ways.

South of the ACC, heat is transported towards the shelves by large cyclonic gyre circulations in the Ross and Weddell sea, which strengthen under global warming. The freshening from ISM additionally accelerates the SPGs and enhances warming of the deep SO. This forms a positive feedback with ISM, as indicated in Fig. 10.

Moreover, the enhanced meridional heat transport south of the ACC weakens the meridional density gradient across the current and dampens the ACC strengthening. But this negative feedback seems to be of minor importance for the heat budget.

Ice shelf melting is limited by local oceanic transport (mainly mixing) of warm water towards the ice shelf. Melt rates in the coupled experiment are reduced, because local cooling of the adjacent ocean is not fully compensated for by additional heat transport towards the coast.

Note that we cannot claim to properly capture even the large-scale oceanic circulation on the continental shelves. Even if our simplified response of ISM to oceanic warming (Sect. 5) would produce realistic melt rates, the parameterization should be forced with a realistic representation of the coastal waters, e.g. the heat exchange across the Antarctic slope front. Generally, coarse resolution models tend to blur tracer gradients. This could lead to both, over- and underestimation of ISM, because neither varying temperature gradients, nor circulation changes will be resolved satisfactorily.

Another question is how quickly the fresh meltwater is rising to the upper ocean layers, where it is less efficient in altering the SPG circulation. Simulations with higher resolution models (Losch 2008; Hellmer 2004) suggest that the freshening signal rises rather quickly within the outer rim of the gyres, which would weaken the mechanism proposed here. In fact, we conducted another simulation with $\alpha = 1$, where ISM fluxes were stopped after 200 years. In this case, the circulation returned within less than five decades to the noISM state.

Similar to the case of the ACC, it is necessary to additionally consider changes in wind stress due to climate change for the SPGs, as well. They may also exceed the buoyancy effects presented within this study.

Nevertheless, our results present a set of ISM effects that will need to be considered, in order to fully understand the future shelf ice–ocean interaction. Hence, they emphasize the importance of a proper representation of ISM effects for a realistic simulation of the SO circulation in climate models.

## References

Alley RB, Clark PU, Huybrechts P, Joughin I (2005) Ice-sheet and sea-level changes. Science 310:456–460. doi:10.1126/science.1114613

Beckmann A, Goosse H (2003) A parametrization of ice shelf-ocean interaction for climate models. Ocean Model 5(2):157–170

Bergamasco A, Defendi V, Zambianchi E, Spezie G (2002) Evidence of dense water overflow ot the ross sea shelf-break. Antarct Sc 14. doi:10.1017/S0954102002000,068

Bi D, Budd WF, Hirst AC, Wu X (2002) Response of the Antarctic circumpolar current transport to global warming in a coupled model. Geophys Res Lett 29(24):3927–3930

Böning C, Dispert A, Visbeck M, Rintoul SR, Schwarzkopf FU (2008) The response of the Antarctic circumpolar current to recent climate change. Nat Geosci 1. doi:10.1038/ngeo362

Born A, Levermann A (2009) The 8k event: abrupt transition of the subpolar gyre towards a modern north atlantic circulation. Nature (in revision)

Borowski D, Gerdes R, Olbers D (2002) Thermohaline and wind forcing of a circumpolar channel with blocked geostrophic contours. J Phys Oceanogr 32:2520–2539

Cavalieri DJ, Parkinson CL, Vinnikov KY (2003) 30-Year satellite record reveals contrasting Arctic and Antarctic sea ice variability. Geophys Res Lett 38. doi:10.1029/2003GL018,031

Cunningham SA, Alderson SD, King BA, Brandon MA (2003) Transport and variability of the Antarctic circumpolar current in drake passage. J Geophys Res 108. doi:10.1029/2001JC001,147

Curran MAJ, Ommen TD, Morgan VI, Palmer KLPAS (2003) Ice core evidence for Antarctic sea ice decline since the 1950s. Science 302. doi:10.1126/science.1087,888

England M (1993) Representing the global-scale water masses in ocean general circulation models. J Phys Oceanogr 23:1523–1552

Fichefet T, Maqueda MAM (1997) Sensitivity of a global sea ice model to the treatment of ice thermodynamics and dynamics. J Geophys Res 102:12609–12646

Fyfe JC, Saenko OA (2006) Simulated changes in the extratropical Southern Hemisphere winds and currents. Geophys Res Lett 33:L06701. doi:10.1029/2005GL025332

Fyfe JC, Saenko OA, Zickfeld K, Eby M, Weaver AJ (2007) The role of poleward intensifying winds on Southern Ocean warming. J Clim (submitted)

Garabato ACN, , Stevens DP, Watson AJ, Roether W (2007) Short-circuiting of the overturning circulation in the Antarctic circumpolar current. Nature 447:194–197. doi:10.1038/nature05832

Gent PR, McWilliams JC (1990) Isopycnal mixing in ocean circulation models. J Phys Oceanogr 20:150–155

Gent PR, Large WG, Bryan FO (2001) What sets the mean transport through drake passage? J Geophys Res 1006:2693–2712

Gill AE (1972) Circulation and bottom water production in the Weddell sea. Deep Sea Res 20:111–140

Gille ST (2002) Warming of the southern ocean since the 1950s. Science 295. doi:10.1126/science.1065,863

Giovinetto MB, Bentley CR (1985) Surface balance in ice drainage system of Antarctica. Antarct JUS 20:6–13

Grosfeld K, Sandhäger H (2004) The evolution of a coupled ice shelf-ocean system under different climate states. Glob Planet Change 42:107–132

Hallberg R, Gnanadesikan A (2006) The role of eddies in determining the structure and response of the wind-driven southern hemisphere overturning: results from the modeling eddies in the southern ocean (meso) project. J Phys Oceanogr 36:2232–2252

Hellmer HH (2004) Impact of Antarctic ice shelf basal melting on sea ice and deep ocean properties. Geophys Res Lett 31. doi:10.1029/2004GL019,506

Holland DM, Jenkins A (1999) Modeling thermodynamic ice–ocean interactions at the base of an ice shelf. J Phys Oceanogr 29:1787–1800

Holland PR, Jenkins A, Holland DM (2008) The response of ice shelf basal melting to variations in ocean temperature. J Clim 21. doi:10.1175/2007JCLI1909.1

Jacobs SS, Giulivi CF, Mele PA (2002) Freshening of the ross sea during the late 20th century. Science 297. doi:10.1126/science.1069,574

Lange MM, Blindow N, Breuer B, Grosfeld K, Kleiner T, Mohrholz CO, Nicolaus M, Oelke C, Sandhäger H, Thoma M (2005) Numerical model studies of Antarctic ice-sheet ice-shelf ocean systems and ice caps. Ann Glaciol 41:111–120

Levermann A, Born A (2007) Bistability of the subpolar gyre in a coarse resolution climate model. Geophys Res Lett 34:L24605. doi:10.1029/2007GL031732

Levermann A, Griesel A (2004) Solution of a model for the oceanic pycnocline depth: scaling of overturning strength and meridional pressure difference. Geophys Res Lett 31:L17302. doi:10.1029/2004GL020678

Levermann A, Griesel A, Hofmann M, Montoya M, Rahmstorf S (2005) Dynamic sea level changes following changes in the thermohaline circulation. Clim Dyn 24:347–354. doi:10.1007/s00382-004-0505-y

Levermann A, Mignot J, Nawrath S, Rahmstorf S (2007a) The role of northern sea ice cover for the weakening of the thermohaline circulation under global warming. J Clim 20:4160–4171

Levermann A, Schewe J, Montoya M (2007b) Lack of bipolar seesaw in response to Southern Ocean wind reduction. Geophys Res Lett 34(12):L12711. doi:10.1029/2007GL030255

Losch M (2008) Modeling ice shelf cavities in a $z$ coordinate ocean general circulation model. J Geophys Res 113. doi:10.1029/2007JC004,368

Manabe S, Stouffer RJ (1980) Sensitivity of a global climate model to an increase of $CO_2$ concentration in the atmosphere. J Geophys Res 85:5529–5554

Mignot J, Levermann A, Griesel A (2006) A decomposition of the Atlantic meridional overturning circulation into physical components using its sensitivity to vertical diffusivity. J Phys Oceanogr 36:636–650

Montoya M, Levermann A (2008) Surface wind-stress threshold for glacial atlantic overturning. Geophys Res Lett 35. doi:10.1029/2007GL032,560

Montoya M, Griesel A, Levermann A, Mignot J, Hofmann M, Ganopolski A, Rahmstorf S (2005) The earth system model of intermediate complexity CLIMBER-3α. Part I: description and performance for present day conditions. Clim Dyn 25:237–263. doi:10.1007/s00382-005-0061-0

Myers P, Fanning A, Weaver A (1996) Jebar, bottom pressure torque, and Gulf Stream separation. J Phys Oceanogr 26:671–683

Nicholls K (1997) Predicted reduction in basal melt rates of an Antarctic ice shelf in a warmer climate. Nature 388:460–462

Olbers D, Borowski D, Vlker C, Wlff J (2004) The dynamical balance, transport and circulation of the Antarctic circumpolar current. Antarct Sci 16. doi:10.1017/S0954102004002,251

Olbers D, Lettmann K, Timmermann R (2006) Six circumpolar currents—on the forcing of the Antarctic circumpolar current by wind an mixing. Ocean Dyn 57. doi:10.1007/s10,236-006-0087-9

Orsi AH, Johnson GC, Bullister JL (1999) Circulation, mixing, and production of Antarctic bottom water. Prog Oceanogr 43:55–109

Payne A, Vieli A, Shepherd AP, Wingham DJ, Rignot E (2004) Recent dramatic thinning of larges west Antarctic ice stream triggered by oceans. Geophys Res Lett 31. doi:10.1029/2004GL021,284

Petoukhov V, Ganopolski A, Brovkin V, Claussen M, Eliseev A, Kubatzki C, Rahmstorf S (2000) CLIMBER-2: a climate system model of intermediate complexity. Part I: model description and performance for present climate. Clim Dyn 16:1

Rahmstorf S, Ganopolski A (1999) Long-term global warming scenarios computed with an efficient coupled climate model. Clim Change 43:353

Rignot E, Jacobs SS (2002) Rapid bottom melting widespread near Antarctic ice sheet grounding lines. Science 296. doi:10.1126/science.1070,942

Rignot E, Casassa G, Gogieneni P, Rivera A, Thomas R (2004) Accelerated ice discharge from the Antarctic peninsular following the collapse of Larsen B ice shelf. Geophys Res Lett 31. doi:10.1129/2004GL020,697

Rignot E, Bamber JL, Broeke MRVD, Davis C, Li Y, Berg WJVD, Meijgaard EV (2008) Recent Antarctic ice mass loss from radar interferometry and regional climate modelling. Nat Geosci 1:106–110. doi:10.1038/ngeo102

Rintoul SR, Sokolv S (2001) Channelized bottom melting and stability of floating ice shelfs. J Geophys Res 106:2815–2832

Rintoul SR, Hughes C, Olbers D (2001) The Antarctic circumpolar current system. In: Siedler G, Church J, Gould J (eds) Ocean circulation and climate: observing and modelling the global ocean, vol 77. Academic Press, New York, pp 271–303

Saenko OA, Weaver AJ (2003) Southern Ocean upwelling and eddies: sensitivity of the global overturning to the surface density range. Tellus 55A:106–111

Saenko OA, Weaver AJ (2004) What drives heat transport in the Atlantic: sensitivity to mechanical energy supply and buoyancy forcing in the Southern Ocean. Geophys Res Lett 31:L20305. doi:10.1029/2004GL020671

Scambos T, Bohlander J, Shuman JA, Skvarca P (2004) Glacier acceleration and thinning after ice shelf collapse in the Larsen B embayment, Antarctica. Geophys Res Lett 31. doi:10.1029/2004GL020,670

Schewe J, Levermann A (2009) The role of meridional density differences for a wind-driven overturning circulation. Clim Dyn (in press). doi:10.1007/s00382-009-0572-1

Schröder M, Fahrbach E (1999) On the structure and the transport of the eastern Weddell gyre. Deep Sea Res II 46:501–527

Smedsrud LH, Jenkins A, Holland DM, Nøst OA (2006) Modeling ocean processes below fimbulisen, Antarctica. Geophys Res Lett 111. doi:10.1029/2005JC002,915

Swingedouw D, Fichefet T, Goosse H, Driesschaert E, Loutre MF (2008a) Antarctic ice-sheet melting provides negative feedbacks on future climate warming. Clim Dyn. doi:10.1007/s00,382-008-0496-1

Swingedouw D, Fichefet T, Hybrechts P, Goosse H, Driesschaert E, Loutre MF (2008b) Antarctic ice-sheet melting provides

negative feedbacks on future climate warming. Geophys Res Lett 35. doi:10.1029/2008GL034,410

Thomas ER, Marshall GR, McConnell JR (2008) A doubling in snow accumulation in the western Antarctic peninsula since 1850. Geophys Res Lett 35. doi:10.1029/2007GL032,529

Toole JM, Polzin KL, Schmitt RW (1994) Estimates of diapycnal mixing in the abyssal ocean. Science 264:1120–1123

Trenberth K, Olson J, Large W (1989) A global ocean wind stress climatology based on ECMWF analyses. Tech. Rep. NCAR/TN-338+STR, National Center for Atmospheric Research, Boulder, Colorado, USA

Walker RT, Holland DM (2007) A two-dimensional coupled model for ice shelf-ocean interaction. Ocean Model 17:123–139

Wang C, Beckmann A (2007) Investigation of the impact of Antarctic ice-shelf melting in a global ice-ocean model (orca2-lim). Ann Glaciol 46:78–82

Wang Z, Meredith MP (2008) Density-driven southern hemisphere subpolar gyres in coupled climate models. Geophys Res Lett 35. doi:10.1029/2008GL034,344

Williams MJM, Jenkins A, Determann J (1998) Physical controls on ocean circulation beneath ice shelves revealed by numerical models. In: Jacobs SJ, Weiss RF (eds) Ocean, ice, and atmosphere: interactions at the Antarctic continental margin, vol 75. American Geophysical Union, Washington D.C., pp 285–299

Williams MJM, Warner RC, Budd WF (2001) Sensitivity of the Amery ice shelf, Antarctica, to changes in the climate of the southern ocean. J Clim 15:2740–2757